2010

CrOx/nano-Ce0.60Zr0.35Y0.05O2 catalysts that are highly selective for the oxidative dehydrogenation of isobutane to isobutene

Guozhi Wang

Hongxing Dai

Lei Zhang

Jiguang Deng

Caixin Liu

See next page for additional authors

Authors
Guozhi Wang, Hongxing Dai, Lei Zhang, Jiguang Deng, Caixin Liu, Hong He, and Chak-Tong Au

CrO_x/*nano*-$Ce_{0.6}Z_{0.35}Y_{0.05}O_2$ catalysts that are highly selective for the oxidative dehydrogenation of isobutane to isobutene

Guozhi Wang[a], Hongxing Dai[a,*], Lei Zhang[a], Jiguang Deng[a], Caixin Liu[a], Hong He[a], and Chak Tong Au[b,†]

[a] *Laboratory of Catalysis Chemistry and Nanoscience, Department of Chemistry and Chemical Engineering, College of Environmental and Energy Engineering, Beijing University of Technology, Beijing 100124, P.R. China*

[b] *Department of Chemistry and Center for Surface Analysis and Research, Hong Kong Baptist University, Kowloon Tong, Hong Kong, P.R. China*

* Corresponding author. E-mail: hxdai@bjut.edu.cn; Tel.: +86-10-6739-6588; fax: +86-10-6739-1983.

† Co-corresponding author. E-mail: pctau@hkbu.edu.hk; Tel.: +852-3411-7067; fax: +852-3411-7348.

Nanosized $Ce_{0.60}Zr_{0.35}Y_{0.05}O_2$ (*nano*-CZY) solid solution with a particle size of 4–5 nm and CrO_x/*nano*-CZY catalysts were prepared. The 8 wt% CrO_x/*nano*-CZY catalyst performs the best, giving 93% isobutene selectivity and 10% isobutene yield at 540°C in isobutane oxidative dehydrogenation. Such an excellent performance is related to the good reducibility of CrO_x domains and the promotion of O_2 adsorption at oxygen vacancies of *nano*-CZY.

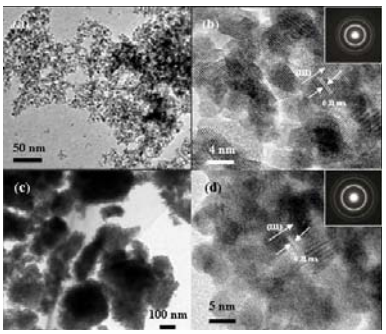

CrO_x/*nano*-$Ce_{0.6}Z_{0.35}Y_{0.05}O_2$ catalysts that are highly selective for the oxidative dehydrogenation of isobutane to isobutene

Guozhi Wang[a], Hongxing Dai[a,*], Lei Zhang[a], Jiguang Deng[a], Caixin Liu[a], Hong He[a], and Chak Tong Au[b,†]

[a] *Laboratory of Catalysis Chemistry and Nanoscience, Department of Chemistry and Chemical Engineering, College of Environmental and Energy Engineering, Beijing University of Technology, Beijing 100124, P.R. China*

[b] *Department of Chemistry and Center for Surface Analysis and Research, Hong Kong Baptist University, Kowloon Tong, Hong Kong, P.R. China*

*Corresponding author: Prof. Hongxing Dai

E-mail: hxdai@bjut.edu.cn

Tel. No.: +86-10-6739-6588

Fax: +86-10-6739-1983

† Co-corresponding author: Prof. Chak Tong Au

E-mail: pctau@hkbu.edu.hk

Tel. No.: +852-3411-7067

Fax: +852-3411-7348.

Abstract

Fluorite-type nanosized $Ce_{0.60}Zr_{0.35}Y_{0.05}O_2$ (*nano*-CZY) solid solution catalysts that are relatively uniform in particle size (4–5 nm) and *y* CrO_x/*nano*-CZY (*y* is the weight percentage of Cr_2O_3 ranging from 2 to 10 wt%) catalysts were prepared by the ethylene glycol-assisted CTAB-templated co-precipitation and incipient wetness impregnation methods, respectively. The materials were characterized by a number of analytical techniques and their catalytic performance was evaluated for the oxidative dehydrogenation of isobutane. The *y* CrO_x/*nano*-CZY catalysts show excellent activities, with the *y* = 8 wt% one performing the best (ca. 93% isobutene selectivity and ca. 10% isobutene yield at 540 ^oC and 30 000 mL/(g_{cat} h)). We conclude that the good reducibility of the highly dispersed CrO_x domains and the promotion of O_2 adsorption at oxygen vacancies of *nano*-CZY (for enhanced oxidation of the reduced catalyst) are responsible for the excellent performance of the 8 wt% CrO_x/*nano*-CZY catalyst.

Keywords: ceria-zirconia-yttria solid solution; nanoparticle; supported chromia catalyst; isobutane oxidative dehydrogenation

1. Introduction

The catalytic conversion of light hydrocarbons to value-added organic compounds is of economic and environmental significance. Compared to the high-temperature nonoxidative dehydrogenation of alkane to alkene, the thermodynamically favorable oxidative dehydrogenation (ODH) pathway is better. This is because the latter can be conducted at much lower temperatures and the inevitable problems of the former such as cracking of hydrocarbons, carbon deposition, and catalyst deactivation can be avoided to a great extent. However, the ODH process usually gives rise to comparatively lower alkene selectivity due to deep oxidation, resulting in a waste of raw material (alkane). Therefore, the design and fabrication of materials that are catalytically selective to alkene formation is the key to effective utilization of light hydrocarbons through the ODH route.

A number of studies have shown that supported vanadia (VO_x) [1,2], chromia (CrO_x) [3], and molybdena (MoO_x) [4] perform well in the ODH of alkane. Investigations have been conducted over catalysts such as Cr-Ce-O [5] and Ca-CrO_x/Al_2O_3 [6]. Yang et al. [4] studied the structure and catalytic properties of V_2O_5/Cr_2O_3/Al_2O_3 and V_2O_5/MoO_3/Al_2O_3 for propane ODH. They observed that the V-O-Cr(Mo) linkage was more reducible and reactive than the V-O-V linkage and the V_2O_5/Cr_2O_3/Al_2O_3 catalysts were more active than the V_2O_5/Al_2O_3 catalysts. Neri et al. [6] studied a series of CaO-modified CrO_x/Al_2O_3 catalysts and found that the 2 wt% Ca-doped CrO_x/Al_2O_3 exhibited a maximum isobutene selectivity of 57% at 7% isobutane conversion due to the formation of well-dispersed Cr^{6+} species.

In the ODH of alkane, the property of a catalyst support is an important factor that influences selectivity and activity [7,8]. It is known that nanometer ceria-zirconia or

ceria-zirconia-yttria solid solutions have two distinct properties: (i) high density of oxygen vacancies, enabling facile activation of O_2 and hydrocarbon molecules, and (ii) good oxygen storage/release ability, facilitating redox actions [9]. As a result, the nanomaterials are good catalyst supports for ODH reactions. On the other hand, the physicochemical properties of CeO_2 or $Ce_{1-x}Zr_xO_2$ can be considerably modified by doping the oxide lattice with suitable metal ions. The partial replacement of Ce by trivalent rare earth metal ions (e.g. La^{3+}, Y^{3+}, or Pr^{3+}) promotes the formation of oxygen vacancies and noticeably improves the thermal stability, redox ability, and OSC (oxygen storage capacity) of the solid solutions [10,11], hence enhancing catalytic performance [12].

Previously, we observed that single transition metal oxides (CrO_x) [13,14] and binary transition metal oxides (CrO_x–MoO_x) [15] could be highly dispersed on the surfaces of ordered nanoporous silica (SBA-15) and MgO-coated 3D nanoporous SBA-16. These materials showed good catalytic activities for the ODH of isobutane [14,15]. We also reported that with the inclusion of a small amount of Y^{3+} in the $RE_{0.6}Zr_{0.4}O_2$ (RE = Ce, Pr) lattice, the as-obtained $RE_{0.6}Zr_{0.35}Y_{0.05}O_2$ solid solutions are enriched with oxygen vacancies, consequently showing enhanced lattice oxygen mobility and oxygen storage/release (redox) ability [9,16]. It is known that the ODH reaction proceeds via a Mars-van Krevelen redox mechanism (with the lattice oxygen of transition metal oxide domains in the supported catalyst involved in the rate-determining steps of C–H bond activation [17]), and the reduced catalyst is re-oxidized by O_2 from the gas phase. We envisage that the unique properties of nanosized ceria-zirconia-based materials are beneficial for ODH reactions. Using nanometer $Ce_{0.60}Zr_{0.35}Y_{0.05}O_2$ solid solution (*nano*-CZY) as support and chromia as active component, we

prepared a series of CrO_x/*nano*-CZY catalysts of different chromia loadings and found that the nanomaterials perform excellently in the ODH of isobutane to isobutene. In this paper, we report the fabrication and catalytic activities of the *nano*-CZY-supported CrO_x catalysts.

2. Experimental

2.1. Catalyst preparation

The *nano*-CZY support was synthesized according to a rather novel strategy. In a typical procedure, stoichiometric amounts of metal precursors (4.5 mmol $Ce(NO_3)_3{\cdot}6H_2O$, 2.6 mmol $ZrO(NO_3)_2{\cdot}2H_2O$, 0.4 mmol $Y(NO_3)_3{\cdot}6H_2O$), hexadecyltrimethyl ammonium bromide (CTAB) and ethylene glycol (EG) surfactants (giving (Ce + Zr + Y)/(CTAB + EG) and CTAB/EG molar ratio of 1/1.2 and 1/600, respectively) were dissolved in 30 mL of deionized water. An ammonia (28 wt%) solution was added dropwise to the mixture under stirring and the pH value was carefully controlled to 11 for the generation of a yellowish precipitate. After being washed three times with deionized water and methanol, the precipitate was filtered out and dried at 80 ^oC for 48 h, thus obtaining the CTAB/EG-removed CZY precursor. The as-generated CZY precursor was heated to 600 ^oC at a rate of 1 °C/min and maintained at this temperature for 2 h for the acquisition of the *nano*-CZY support.

The *y* CrO_x/*nano*-CZY (*y* represents the Cr_2O_3 weight percentage, *y* = 2, 4, 6, 8, or 10 wt%) catalysts were prepared through the incipient wetness impregnation of *nano*-CZY with suitable amount of $Cr(NO_3)_3$ solution. The dried precursor was calcined (heated from room temperature (RT) to 550 ^oC at a ramp of 10 ^oC/min) in O_2 (30 mL/min) at 550 ^oC for 3 h. Finally, the as-received solid substance was ground, pressed, crushed, and sieved to a size

range of 40−60 mesh. For comparison purposes, we adopted the incipient wetness impregnation approach to prepare a γ-Al_2O_3 (surface area = 104 m^2/g) supported chromia catalyst (8 wt% CrO_x/Al_2O_3, Cr surface density = 8.45 Cr/nm^2). All the chemicals were analytical grade (Beijing Chemical Reagent Co.) and were used without further purification.

2.2. Catalyst characterization

X-ray diffraction (XRD) patterns of the *nano*-CZY and *y* CrO_x/*nano*-CZY samples were recorded on a Bruker/AXS D8 Advance diffractometer using Cu $K\alpha$ irradiation and nickel filter (λ = 0.15406 nm). The BET surface areas of the samples were measured by means of a Micromeritics ASAP 2020 instrument. Before the adsorption of N_2 at −196 ^oC, the samples were degassed at 250 ^oC for 3 h. The transmission electron microscopic (TEM) images and selected area electron diffraction (SAED) patterns of the samples were taken on a JEOL-2010 apparatus operated at a 200 kV accelerating voltage. The X-ray photoelectron spectroscopic (XPS, VG CLAM 4 MCD analyzer) technique was applied to determine the O 1s, Cr 2p, Ce 3d, Zr 3d, Y 3d, and C 1s binding energies (BEs) of surface oxygen, chromium, cerium, zirconium, yttrium, and carbon species using Mg $K\alpha$ ($h\nu$ = 1253.6 eV) as excitation source. Before XPS measurements, the samples were pretreated in an O_2 flow of 20 mL/min at 500 ^oC for 1 h and then cooled to RT. Then the samples were mounted and transferred to the spectrometer in a transparent Glove Bag (Instruments for Research and Industry, USA) filled with helium. Finally, the samples were outgassed (in the preparation chamber) for 0.5 h before XPS analysis. The BE values were calibrated against the C 1s signal (284.6 eV) of contaminant carbon. Raman spectra of the *y* CrO_x/*nano*-CZY samples were collected on a laser Raman instrument (Bruker RFS/100) equipped with a Nd:YAG laser (1064 nm) and an

InGaAs detector. The laser power was 100 mW. For each Raman run, the sample (0.2 g) was mounted inside the Raman cell on a stainless steel holder and Raman scattering (in the 200−1200 cm^{-1} region) was collected with 4 cm^{-1} resolution.

H_2 temperature-programmed reduction (H_2-TPR) was carried out in the RT−700 ^oC range. About 50 mg of sample was treated in O_2 (40 mL/min) at 500 ^oC for 1 h and then cooled down to RT before being reduced in a 5% H_2−95% He flow of 25 mL/min at a ramp rate of 10 ^oC/min. The effluent was monitored with a mass spectrometer (MS, Hiden HPR20), and the MS response was calibrated against the complete reduction of a standard CuO powder sample (99.995%, Aldrich).

2.3. Catalytic evaluation

The ODH of isobutane (i.e. *i*-butane or *i*-C_4H_{10}) was performed in a quartz fixed-bed micro-reactor at atmospheric pressure and a feed gas (*i*-$C_4H_{10}/O_2/N_2$ molar ratio = 2 : 4 : 44) flow rate of 50 mL/min. Unless specified otherwise, 0.1 g of the catalyst (40–60 mesh) was used (diluted with an equal amount of acid-washed quartz sand (40–60 mesh) to minimize the temperature gradient), giving a space velocity (SV) of 30 000 mL/(g_{cat} h). A thermocouple was placed in the middle of the catalyst bed to measure the reaction temperature. The effluent was analyzed on-line using a Shimadzu GC-2010 gas chromatograph equipped with FID and TCD. The aluminum oxide porous layer open tubular (Rt-Alumina PLOT, Restek, USA) capillary column (30 m in length, for FID) was used to separate hydrocarbons, whereas the Uni Beads-1S column (3 m in length, for TCD) was used to separate CO, CO_2, and O_2. The isobutane conversion and product selectivity were calculated based on carbon balance.

To clarify the effect of oxygen adspecies on catalytic performance, we performed

isobutane-pulse (50.0 μL for each pulse) experiments at 340 ^{o}C over the 8 wt% CrO_x/*nano*-CZY catalysts (0.1 g) using helium (flow rate = 30 mL/min) as carrier gas. Before each experiment, the catalyst was in-situ pretreated in an O_2 or H_2 flow of 30 mL/min at 350 ^{o}C for 0.5 h, and then purged with helium for 0.5 h. The outlet gases were analyzed on-line by GC-MS (Agilent 5975B).

3. Results and discussion

3.1. Crystal phase composition, BET surface area, and pore structure

Figure 1 shows the wide-angle XRD patterns of the *nano*-CZY and *y* CrO_x/*nano*-CZY samples. By comparing to the XRD patterns of cubic $Ce_{0.6}Zr_{0.4}O_2$ (JCPDS PDF# 38-1439), one can realize that the as-fabricated *nano*-CZY is of fluorite-type cubic crystal structure, indicating the formation of single-phase CZY solid solution [9]; all the peaks can be indexed as shown in Fig. 1(a). With loading of CrO_x, there is little change in CZY line position, demonstrating the retention of the cubic structure; the only observable change is a drop in peak intensity, implying a decline in CZY crystallinity. When chromia loading reaches 10 wt% (Fig. 1(f)), weak signals ascribable to α-Cr_2O_3 crystal phase (JCPDS PDF# 02-1095) are detected. The results suggest that at loadings < 10 wt%, the CrO_x domains are highly dispersed on the *nano*-CZY surfaces. The BET results indicate that the surface area of the catalysts is 100, 74, 74, 72, 73, and 70 m^2/g for *y* = 0, 2, 4, 6, 8, and 10 wt%, respectively. The corresponding Cr surface density values (i.e. the number of Cr atoms per nm^2 surface area) are 0, 2.26, 4.33, 6.60, 8.66, and 10.74 Cr/nm^2. It should be noted that if all the CZY particles were spherical with a diameter of 5 nm, the surface area of CZY would be ca. 160 m^2/g (CZY density = ca. 7.5

g/cm^3), much higher than that of the as-fabricated CZY sample. The result means that the CZY particles are not perfectly spherical. Therefore, we describe them as sphere-like particles.

Figure 2 shows the representative TEM images and SAED patterns of *nano*-CZY and 8 wt% CrO_x/*nano*-CZY. The *nano*-CZY sample displays a picture of irregular clusters, each cluster is composed of a number of relatively uniform sphere-like CZY nanoparticles (diameter: 4–5 nm) (Fig. 2(a,b)). There are a large number of nanopores between the CZY nanoparticles (Fig. 2(b)). After 8 wt% chromia is loaded on the *nano*-CZY support, the aggregation of CZY nanoparticles becomes serious (Fig. 2(c)) but there is little change in the size of nanoparticles (Fig. 2(d)). The appearance of multiple bright electron diffraction rings in the SAED patterns (insets of Figs. 2(b,d)) reveals that the as-obtained *nano*-CZY and 8 wt% CrO_x/*nano*-CZY materials are polycrystalline. The recording of well-resolved lattice fringes (Figs. 2(b,d)) indicates the generation of well-grown CZY solid solution. The lattice spacing is measured to be ca. 0.31 nm, coinciding with that (0.312485 nm) of the (111) plane of cubic CeO_2 (JCPDS PDF# 81-0792) or that (0.306400 nm) of the (111) plane of cubic $Ce_{0.6}Zr_{0.4}O_2$ (JCPDS PDF# 38-1439).

3.2. Surface species and reducibility

Figure 3 illustrates the O 1s, Ce 3d, and Cr 2p XPS spectra of *y* CrO_x/*nano*-CZY. In Fig. 3(A), one can see unsymmetrical O 1s peaks at BE = ca. 529.5 eV that can be divided into two components by deconvolution: one at 529.4 eV and the other at 531.6 eV. The former is attributable to surface lattice oxygen while the latter is attributable to adsorbed oxygen (e.g. O_2^-, O_2^{2-} or O^-) species [18,19]. The presence of surface hydroxyl group species can be excluded because the samples were pretreated in O_2 at 500 ^oC and were not exposed to air prior

to XPS analysis. Due to the fact that the O 1s BEs of α-Cr_2O_3 and mono-/poly-chromate are in the range of 529–530 eV, it is not possible to exclude the co-existence of α-Cr_2O_3 and CrO_x domains, especially at high chromia loadings. In Fig. 3(B), one can see two sets of Ce 3d signals: one has peaks at BE = 882.8, 885.4, 889.1, and 898.7 eV attributable to Ce $3d_{5/2}$ while the other has peaks at BE = 901.8, 903.4, 907.6, and 917.0 eV attributable to Ce $3d_{3/2}$ [20,21]. The signals at BE = 885.4 and 903.4 eV are due to Ce^{3+} while the others due to Ce^{4+} [20,21]. In other words, the cerium of *nano*-CZY and *y* CrO_x/*nano*-CZY existed either as Ce^{3+} or as Ce^{4+}. The co-existence of Ce^{3+} and Ce^{4+} ions in *y* CrO_x/*nano*-CZY suggests the presence of oxygen vacancies on/in the *nano*-CZY support. It is known that oxygen vacancies are apt to promote O_2 adsorption and activation, consequently facilitating the $Ce^{3+} \Leftrightarrow Ce^{4+}$ redox process [9,16]. The formation of oxygen vacancies in $Ce_{1-x}Zr_xO_2$ has been reported by Balducci et al. [22] and Madier et al. [23], and enhanced density of oxygen vacancies via Y^{3+} doping to the lattice of ceria-zirconia solid solution has been reported by He et al. [9] and Cavani et al. [24]. Usually, O_2 molecules are adsorbed at oxygen vacant sites, and it is reasonable to believe that the oxygen adspecies are largely located on the *nano*-CZY surface of the *y* CrO_x/*nano*-CZY catalysts. As illustrated in Fig. 3(C), the two asymmetrical Cr 2p peaks can be deconvoluted into two sets of components: one with peaks at 576.9 and 579.0 eV, and the other with peaks at 586.0 and 588.2 eV. The signals at ca. 576.9 and 586.0 eV can be assigned to Cr^{3+} whereas those at ca. 579.0 and 588.2 eV can be assigned to Cr^{6+} [24,25].

The surface O_{ads}/O_{latt}, Ce^{3+}/Ce^{4+}, and Cr^{6+}/Cr^{3+} ratios as depicted in Table 1 were calculated according to peak areas. One can see that, with rise of chromia content, there is only a slight increase in the amounts of oxygen adspecies and surface Ce^{3+} species, indicating that

the loading of chromia on *nano*-CZY does not cause a significant change in the density of surface oxygen vacancies. One the other hand, with increase of chromia loading, there is a monotonous decline in the amount of surface Cr^{6+} species.

As a potent tool to obtain structural information, laser Raman is sensitive to crystalline symmetry. Illustrated in Fig. 4 are the laser Raman spectra of the *y* CrO_x/*nano*-CZY samples. The Raman spectrum of *nano*-CZY (not shown here) and that of the *nano*-CZY in *y* CrO_x/*nano*-CZY shows a big band at 460 cm^{-1} and a weak band at 600 cm^{-1}. The former corresponds to a triply degenerate F_{2g} mode and can be viewed as a mode of symmetric O–Ce–O stretching [25], whereas the latter can be ascribed to a doubly degenerate longitudinal optical mode of ceria-zirconia-yttria (similar to that of CeO_2 [26]) and linked to oxygen vacancies in the lattices of solid solutions [27]. In the present investigation, we detected no Raman bands ascribable to zirconia or yttria phases. The results reveal that the Zr^{4+} and Y^{3+} ions are incorporated into the CeO_2 lattices. In other words, there is the generation of single-phase CZY solid solutions. It is generally accepted that there are three kinds of chromium species on the surface of supported chromia, *viz*. isolated monochromate (CrO_3), polychromate α-Cr_2O_3, and crystalline α-Cr_2O_3. In Fig. 4, one can observe Raman bands at 850, 875, 980, and 1009 cm^{-1}: the first two can be assigned to Cr-O-Cr stretching of hydrated dichromate [28], the third to monochromate species of Cr^{6+} state (CrO_3) [4], and the fourth to polychromate species with different degrees of oligomerization [4,28]. With the rise of chromia loading from 2 to 6 wt% (Figs. 4(a–c)), the Raman bands increase in intensity, indicative of an increase in content of chromium species, but further rise of chromia loading to 8 or 10 wt% results in a decline in signal intensity, plausibly due to the formation of

crystalline α-Cr_2O_3 [29] as evidenced by the observation of Raman bands at 550 cm^{-1} (Figs. 4(d, e)). Based on the Raman results, one can deduce that near monolayer coverage of chromia on *nano*-CZY surface is achieved at a chromia loading of ca. 8 wt% (corresponding to a Cr surface density of ca. 8.66 Cr/nm^2); at this stage the formation of crystalline α-Cr_2O_3 should be minimal.

Most researchers believe that the ODH of alkanes over supported transition metal oxides proceeds via a redox mechanism and the reducibility of the catalyst plays a crucial role. Shown in Figs. 5A and B are the H_2-TPR profiles and initial H_2 consumption rates of *y* CrO_x/*nano*-CZY, respectively. For *nano*-CZY (not shown), there is a broad and weak reduction band centered at 505 ^oC due to the removal of oxygen adspecies and the reduction of surface Ce^{4+} to Ce^{3+} [30], corresponding to a H_2 consumption of 0.83 mmol/g_{cat}. With the loading of chromia, the *y* CrO_x/*nano*-CZY samples show a strong reduction band in the 280–420 ^oC range, together with a broad and weak reduction band centered at 493 ^oC. The former is due to the reduction of chromia, whereas the latter is due to the reduction of Ce^{4+} ions in *nano*-CZY. The slight drop in reduction extent of the *nano*-CZY support of *y* CrO_x/*nano*-CZY with the rise of chromia loading could be a result of strong interaction between *nano*-CZY and CrO_x domains. At elevated chromia loadings, the shift (to lower temperature) of the reduction band of chromia becomes prominent. It might be a combined result of (i) the presence of highly dispersed CrO_x domains that are reducible and (ii) the strong interactions between CrO_x and CZY nanocrystals. A similar effect was also observed in the case of VO_x/Al_2O_3 by Dai et al. [2]. The H_2 consumption for the reduction of CrO_x in *y* CrO_x/*nano*-CZY at *y* = 2, 4, 6, 8, and 10 wt% is 0.27, 0.50, 0.71, 0.92, and 0.87 mmol/g_{cat},

respectively, corresponding to a Cr^{6+} content of 89, 83, 78, 76, and 58 mol%, higher than the respective surface Cr^{6+} content (80, 69, 59, 54, and 51 mol%) estimated based on the surface Ce^{6+}/Cr^{3+} ratios depicted in Table 1. This result is understandable because the amounts of surface and bulk Cr^{6+} concentrations vary across the *nano*-CZY-supported chromia catalysts. The *nano*-CZY in the *y* CrO_x/*nano*-CZY samples shows similar extents of H_2 consumption (0.63, 0.63, 0.62, 0.61, and 0.60 mmol/g_{cat}, respectively). It is obvious that the 8 wt% CrO_x/*nano*-CZY catalyst is the most reducible. The formation of crystalline α-Cr_2O_3 phase causes a drop in H_2 consumption even though the chromia loading of 10 wt% CrO_x/*nano*-CZY is higher than that of 8 wt% CrO_x/*nano*-CZY. It is convenient to use the initial H_2 consumption (where consumption of lattice oxygen is less than 25% and there is no phase transformation of catalyst) rate to evaluate the reducibility of a solid oxide catalyst [2,17]. From Fig. 5B, one can see that the initial H_2 consumption rate basically followed a sequence of 2 wt% CrO_x/*nano*-CZY < 4 wt% CrO_x/*nano*-CZY < 6 wt% CrO_x/*nano*-CZY < 10 wt% CrO_x/*nano*-CZY < 8 wt% CrO_x/*nano*-CZY, indicating that the 8 wt% CrO_x/*nano*-CZY catalyst is the highest in reducibility.

3.3. Catalytic performance

According to the results of blank experiments conducted under similar conditions, *nano*-CZY by itself (at 540 ^oC: isobutane conversion = 21.9%, isobutene selectivity = 2.9%, C_1–C_3 selectivity = 2.4%, and CO_x (CO_2 + CO) selectivity = 94.7%) is highly active for the deep oxidation of isobutane to CO_x, whereas quartz sand (at 540 ^oC: isobutane conversion = 1.1%, isobutene selectivity = 98.1%) is rather inactive but selective. Table 2 summarizes the

catalytic activities of *y* CrO_x/*nano*-CZY under the conditions of isobutane/oxygen molar ratio = 1/2, reaction temperature = 340–540 °C, and SV = 30 000 mL/(g_{cat} h). In the adopted temperature range, O_2 conversions are below 45%. Over the catalysts, with 2 wt% CrO_x/*nano*-CZY being an exception, the rise of reaction temperature causes an increase of isobutane conversion and C_4-olefin yield, accompanied by a decrease in C_4-olefin selectivity and a monotonous increase in C_1–C_3 hydrocarbon selectivity. In the case of 2 wt% CrO_x/*nano*-CZY, isobutane conversion, CO_x selectivity, and C_4-olefin yield alter only slightly with temperature rise. High C_4-olefin yield of ca. 10% is achieved over the 6–10 wt% CrO_x/*nano*-CZY catalysts at 540 °C, corresponding to isobutane conversion and C_4-olefin selectivity of ca. 11% and 91–93%, respectively. Among the generated C_1–C_3 hydrocarbons, the major compound is propylene (ca. 89%) and the others (ca. 11%) are methane, ethane, ethylene, and propane; among the C_4-olefins, the main one is isobutene (ca. 96%) and the others (ca. 4%) are *trans*- and *cis*-butene and butadiene. In addition to these products, there is a trace amount (ca. 0.2%) of C_4-oxygenates (such as alcohol, aldehyde, carboxylic acid) generated at temperatures above 500 °C.

The catalytic activities over the 6–10 wt% CrO_x/*nano*-CZY catalysts (C_4-olefin selectivity > 91% and C_4-olefin yield ≈ 10% at 540 °C) are much better than those achieved over K-CrO_x/SiO_2 (C_4-olefin yield ≈ 6% at 525 °C) [31] and over [Si,V]-MCM-41 (C_4-olefin yield ≈ 5% at 550 °C) [32]. For better comparison, we measured the catalytic activity of 8 wt% CrO_x/Al_2O_3 under similar reaction conditions. At isobutane/oxygen molar ratio = 1/2, reaction temperature = 540 °C, and SV = 30 000 mL/(g_{cat} h), the 8 wt% CrO_x/Al_2O_3 catalyst shows an isobutane conversion of ca. 50% and an isobutene selectivity of ca. 12%, giving a

isobutene yield of ca. 6%. Apparently, the 8 wt% CrO_x/*nano*-CZY catalyst is superior to the 8 wt% CrO_x/Al_2O_3 catalyst in performance. The excellent catalytic performance of the former can be associated with the high dispersion of CrO_x domains on the *nano*-CZY solid solution and the relatively facile activation of O_2 molecules over the catalyst. The fact that the isobutane conversion changes insignificantly with the rise in temperature might be due to a complicated effect induced by the competing reactions (i.e. selective and complete oxidation of isobutene, respectively, by the CrO_x lattice oxygen and the oxygen adspecies at the oxygen vacancies of *nano*-CZY). It is generally accepted that the lattice oxygen of MO_x (M = V, Mo, Cr) domains highly dispersed on a support is the active species for the selective oxidation of light hydrocarbons (e.g., propane and butane [2,17,33,34]), whereas the adsorbed oxygen species are responsible for the deep oxidation of alkanes. In the present work, the lattice oxygen atoms of CrO_x react with isobutane to generate the isobutanoxide intermediates (a mechanism similar to that of propane ODH over VO_x/ZrO_2 [33]) or isobutyl intermediates (a mechanism similar to that of n-butane ODH over supported vanadia [8,34]); both intermediates subsequently decompose to form isobutene. The gas-phase O_2 molecules are adsorbed at the oxygen vacancies of *nano*-CZY, and the oxygen adspecies in the vicinity of the CrO_x domains can effectively re-oxidize the catalysts reduced due to the consumption of CrO_x lattice oxygen (O_{latt}^{2-}) in the ODH process. Consequently, the steps of O_2 (in gas phase) $\rightarrow 2O_{ads}$ (at oxygen vacancies of *nano*-CZY) $\rightarrow 2O_{latt}^{2-}$ (in CrO_x) are promoted. The timely replenishment of the catalyst with O_{latt}^{2-} in CrO_x would guarantee the high selectivity to isobutene. In the meantime, the oxygen adspecies can also oxidize isobutane directly to isobutene as well as to carbon oxides. In other words, the isobutene selectivity is determined

by the relative extent of the ODH and deep oxidation reactions. Due to the limited presence of oxygen vacancies in *nano*-CZY, the amount of oxygen adspecies formed on the CZY surface is low. Taking these results into consideration and based on the activity data, one can realize that the selective oxidation of isobutane is the dominant process, and hence a rise of reaction temperature would only cause a slight increase in isobutane conversion. It is generally accepted that O_{ads} is highly reactive towards light alkanes, resulting in deep oxidation and low olefin selectivity as in the case of *nano*-CZY. Nonetheless, compared to alumina, *nano*-CZY is more suitable to disperse chromia. To clarify the role of oxygen adspecies in the catalytic system, we carried out isobutane-pulse experiments at 340 ^{o}C over the 8 wt% CrO_x/*nano*-CZY catalysts that had been in-situ treated in an O_2 or H_2 flow of 30 mL/min at 350 ^{o}C. The results are summarized in Table 3. Over the oxidized catalyst and with the rise of pulse number, isobutane conversion decreases (reflecting the gradual decrease of oxygen adspecies on *nano*-CZY) while isobutene selectivity increases (implying that with the depletion of oxygen adspecies on *nano*-CZY, CrO_x lattice oxygen becomes significantly involved in the ODH process). Over the reduced catalyst (with most of the oxygen adspecies removed), isobutane conversion is low while isobutene selectivity is high, and there is little change in the two factors with the rise of pulse number. The results indicate that, after pre-reduction of catalyst, interaction of isobutane with lattice oxygen of CrO_x dominates. Another piece of supporting evidence is that, after 25 pulses of isobutane and 25 pulses of O_2 over the reduced catalyst (Table 3), the catalyst (re-oxidized) shows low isobutane conversion and high isobutene selectivity, and the isobutane conversion decreases while the isobutene selectivity increases with the rise of pulse number; the results confirm the involvement of

oxygen adspecies in the replenishment of the reduced catalyst with lattice oxygen. Although the activity measurements of the pulsing experiments were carried out in a non-steady state, useful information can be deduced based on the trend of performance change. It is apparent that the CrO_x lattice oxygen of the *nano*-CZY-supported catalyst is active for isobutane ODH and the oxygen species adsorbed on *nano*-CZY can replenish the reduced catalyst with lattice oxygen (thus promoting the ODH reaction).

Based on the above results and discussion, we deduce that the excellent catalytic performance of the 6−10 wt% CrO_x/*nano*-CZY catalysts is a combined result of (i) presence of highly dispersed CrO_x domains, (ii) better reducibility of catalysts, and (iii) involvement of oxygen adspecies on *nano*-CZY in the re-oxidation of the reduced chromia catalyst.

4. Conclusions

Nanostructured *nano*-CZY support (4−5 nm) and *y* CrO_x/*nano*-CZY (*y* = 2−10 wt%) catalysts were synthesized by ethylene glycol-assisted CTAB-templated and incipient wetness impregnation methods, respectively. The *y* CrO_x/*nano*-CZY catalysts show excellent activities for isobutane ODH, with the 8 wt% CrO_x/*nano*-CZY one performing the best (ca. 93% isobutene selectivity and ca. 10% isobutene yield at 540 ^oC and 30 000 mL/(g_{cat} h)). It is deduced that the excellent catalytic performance is attributable to factors such as (i) existence of highly dispersed CrO_x domains, (ii) better CrO_x reducibility, and (iii) promoted oxidation of the reduced catalysts by oxygen adspecies on *nano*-CZY.

Acknowledgements

The work was supported by the NSF of China (Grant Nos. 20973017 and 20473006), the PHR200907105 of the Beijing Municipal Commission of Education, and the SRF for ROCS (State Education Ministry of China). CTA thanks the Hong Kong Baptist University for financial support.

References

[1] V.V. Chesnokov, A.F. Bedilo, D.S. Heroux, I.V. Mishakov, K.J. Klabunde, J. Catal. 218 (2003) 438–446.

[2] H.X. Dai, A.T. Bell, E. Iglesia, J. Catal. 221 (2004) 491–499.

[3] A. Hakuli, A. Kytökivi, A.I. Krause, T. Suntola, J. Catal. 161 (1996) 393–400.

[4] S. Yang, E. Iglesia, A.T. Bell, J. Phys. Chem. B 109 (2005) 8987–9000.

[5] P. Moriceau, B. Grzybowska, L. Gengembre, Y. Barbaux, Appl. Catal. A: Gen. 199 (2000) 73–82.

[6] G. Neri, A. Pistone, S. De Rossi, E. Rombi, C. Milone, S. Galvagno, Appl. Catal. A: Gen. 260 (2004) 75–86.

[7] T. Blasco, J.M. López Nieto, A. Dejoz, M.I. Vázquez, J. Catal. 157 (1995) 271–282.

[8] T. Blasco, J.M. López Nieto, Appl. Catal. A: Gen. 157 (1997)117–142.

[9] H. He, H.X. Dai, K.W. Wong, C.T. Au, Appl. Catal. A: Gen. 251 (2003) 61–74.

[10] R. Si, Y.-W. Zhang, L.-M. Wang, S.-J. Li, B.-X. Lin, W.-S. Chu, Z.-Y. Wu, C.-H. Yan, J. Phys. Chem. C 111 (2007) 787–794.

[11] C.K. Narula, L.P. Haack, W. Chun, H.-W. Jen, G.W. Graham, J. Phys. Chem. B 103 (1999) 3634–3639.

[12] P. Fang, M.-F. Luo, J.-Q. Lu, S.-Q. Cen, X.-Y. Yan, X.-X. Wang, Thermochim. Acta 478 (2008) 45–50.

[13] L. Zhang, Y.H. Zhao, H.X. Dai, H. He, C.T. Au, Catal. Today 131 (2008) 42–54.

[14] G.Z. Wang, L. Zhang, J.G. Deng, H.X. Dai, H. He, C.T. Au, Appl. Catal. A: Gen. 355 (2009) 192–201.

[15] L. Zhang, J.G. Deng, H.X. Dai, C.T. Au, Appl. Catal. A: Gen. 354 (2009) 72–81.

[16] H. He, H.X. Dai, L.H. Ng, K.W. Wong, C.T. Au, J. Catal. 206 (2002) 1–13.

[17] K.D. Chen, E. Iglesia, A.T. Bell, J. Catal. 192 (2000) 197–203.

[18] A. Galtayries, R. Sporken, J. Riga, G. Blanchard, R. Caudano, J. Electron. Spectrosc. Relat. Phenom. 88–91 (1998) 951–956.

[19] L. Zhu, J. Yu, X. Wang, J. Hazard. Mater. 140 (2007) 205–210.

[20] E. Wuilloud, B. Delley, W.-D. Schneider, Y. Baer, Phys. Rev. Lett. 53 (1984) 202–205.

[21] C. Ho, J.C. Yu, T. Kwong, A.C. Mak, S. Lai, Chem. Mater. 17 (2005) 4514–4522.

[22] G. Balducci, J. Kašpar, P. Fornasiero, M. Graziani, M.S. Islam , J.D. Gale, J. Phys. Chem. B 101 (1997) 1750–1753.

[23] Y. Madier, C. Descorme, A.M. Le Govic, D. Duprez, J. Phys. Chem. B 103 (1999) 10999–11006.

[24] F. Cavani, M. Koutyrev, F. Trifiro, A. Bartolini, D. Ghisletti, R. Iezzi, A. Santucci, G. Del Piero, J. Catal. 158 (1996) 236–250.

[25] X.-M. Lin, L.-P. Li, G.-S. Li, W.-H. Su, Mater. Chem. Phys. 69 (2001) 236–240.

[26] J.E. Spanier, R.D. Robinson, F. Zhang, S.-W. Chan, I.P. Herman, Phys. Rev. B 64 (2001) 245407.

[27] M. Yashima, H. Arashi, M. Kakihana, M. Yoshimura, J. Am. Ceram. Soc. 77 (1994) 1067−1071.

[28] M.A. Vuurman, F.D. Hardcastle, I.E. Wachs, J. Mol. Catal. 84 (1993) 193−205.

[29] M. Cherian, M.S. Rao, A.M. Hirt, I.E. Wachs, G. Deo, J. Catal. 211 (2002) 482−495.

[30] G. Jacobs, U.M. Graham, E. Chenu, P.M. Patterson, A. Dozier, B.H. Davis, J. Catal. 229 (2005) 499−512.

[31] R. Grabowski, B. Grzybowska, J. Słoczyńki, K. Wcisło, Appl. Catal. A: Gen. 144 (1996) 335−341.

[32] B. Sulikowski, Z. Olejniczak, E. Wloch, J. Rakoczy, R.X. Valenzuela, V.C. Corberán, Appl. Catal. A: Gen. 232 (2002) 189−202.

[33] K.D. Chen, A. Khodakov, J. Yang, A.T. Bell, E. Iglesia, J. Catal. 186 (1999) 325−333.

[34] J.M. López Nieto, P. Concepión, A. Dejoz, H. Knözinger, F. Melo, M.I. Vázquez, J. Catal. 189 (2000) 147−157.

Captions of Tables and Figures

Table 1. Surface O_{ads}/O_{latt}, Cr^{6+}/Cr^{3+}, and Ce^{3+}/Ce^{4+} ratios of *y* CrO_x/*nano*-CZY catalysts estimated according to the XPS results

Table 2. Catalytic activities of *y* CrO_x/*nano*-CZY for the ODH of isobutane at isobutane/oxygen molar ratio = 1/2 and SV = 30 000 mL/(g_{cat} h)

Table 3. Isobutane conversions and isobutene selectivities obtained in the isobutane-pulsing experiments at 340 ^oC over the O_2- and H_2 pretreated 8 wt% CrO_x/*nano*-CZY catalysts

Fig. 1. XRD patterns of *y* CrO_x/*nano*-CZY samples with *y* = (a) 0, (b) 2, (c) 4, (d) 6, (e) 8, and (f) 10 wt%.

Fig. 2. TEM images and SAED patterns (insets) of (a, b) *nano*-CZY and (c, d) 8 wt% CrO_x/*nano*-CZY.

Fig. 3. (A) O 1s, (B) Ce 3d, and (C) Cr 2p XPS spectra of *y* CrO_x/*nano*-CZY with *y* = (a) 2, (b) 4, (c) 6, (d) 8, and (e) 10 wt%.

Fig. 4. Laser Raman spectra of *y* CrO_x/*nano*-CZY with *y* = (a) 2, (b) 4, (c) 6, (d) 8, and (e) 10 wt%.

Fig. 5. (A) H_2-TPR profiles and (B) H_2 consumption rate of *y* CrO_x/*nano*-CZY with *y* = (a) 2, (b) 4, (c) 6, (d) 8, and (e) 10 wt%.

Table 1

Surface O_{ads}/O_{latt}, Cr^{6+}/Cr^{3+}, and Ce^{3+}/Ce^{4+} ratios of *y* CrO_x/*nano*-CZY catalysts estimated according to the XPS results

y (wt%)	Surface O_{ads}/O_{latt} ratio	Surface Cr^{6+}/Cr^{3+} ratio	Surface Ce^{3+}/Ce^{4+} ratio
2	0.51	3.91	0.10
4	0.54	2.23	0.11
6	0.57	1.47	0.12
8	0.58	1.18	0.14
10	0.57	1.04	0.13

Table 2

Catalytic activities of *y* CrO_x/*nano*-CZY for the ODH of isobutane at isobutane/oxygen molar ratio = 1/2 and SV = 30 000 mL/(g_{cat} h)

y (wt%)	Temperature	Conversion (%)		Selectivity [a] (%)				Isobutene yield
	(^oC)	isobutane	O_2	isobutene	C_1–C_3	CO_x	$C_4^=$	(%)
2	340	8.9	31.5	95.9	0.5	3.2	0.4	8.5
	460	9.1	33.2	94.5	1.4	3.5	0.6	8.6
	540	9.1	32.5	91.1	4.5	3.4	0.9	8.3
4	340	8.3	28.7	94.8	0.7	4.0	0.4	7.9
	460	9.2	33.9	93.8	1.5	3.9	0.8	8.6
	540	9.9	37.5	92.0	3.1	3.9	1.1	9.2
6	340	8.4	29.4	94.5	0.7	4.2	0.6	7.9
	460	9.4	35.7	93.9	1.6	3.7	0.9	8.9
	540	10.5	41.2	91.7	3.7	3.7	0.9	9.7
8	340	8.1	28.6	94.4	0.8	4.5	0.3	7.6
	460	9.4	34.5	93.8	1.5	3.7	1.0	8.8
	540	11.0	43.8	93.2	2.4	3.5	1.0	10.2
10	340	8.1	30.0	93.1	0.9	4.2	1.8	7.6
	460	9.4	35.0	92.3	2.7	3.4	1.6	8.7
	540	11.1	44.5	90.6	3.8	2.9	2.7	10.0

[a] C_1–C_3 denotes CH_4 + C_2H_6 + C_2H_4 + C_3H_8 + C_3H_6; CO_x = CO_2 + CO; $C_4^=$ denotes 1,3-butadiene + *cis*-2-butene + *trans*-2-butene; in addition, there is a trace amount of C_4-oxygenates in the product mixture.

Table 3

Isobutane conversions and isobutene selectivities obtained in the isobutane-pulsing experiments at 340 ^{o}C over the O_2- and H_2 pretreated 8 wt% CrO_x/*nano*-CZY catalysts

Catalyst	Pulse number											
	1	5	10	15	20	25	26	30	35	40	45	50
O_2-pretreated 8 wt% CrO_x/*nano*-CZY	4.22/79.6 [a]	4.03/81.3	3.71/82.8	3.61/85.6	3.49/88.9	3.28/90.9	3.19/92.0	3.01/93.8	2.74/95.7	2.59/95.8	2.59/95.8	2.58/95.7
H_2-pretreated 8 wt% CrO_x/*nano*-CZY	1.02/99.5	0.76/98.9	0.51/99.1	0.31/99.2	0.13/98.7	0/–	1.86/93.2 [b]	1.12/95.7 [b]	0.76/96.2 [b]	0.41/96.7 [b]	0.18/97.4 [b]	0/– [b]

[a] The data of isobutane conversion (%)/isobutene selectivity (%);

[b] The data were obtained after a pulse of isobutane over the H_2-pretreated catalyst that had undergone 25 pulses of isobutane and 25 pulses of O_2.

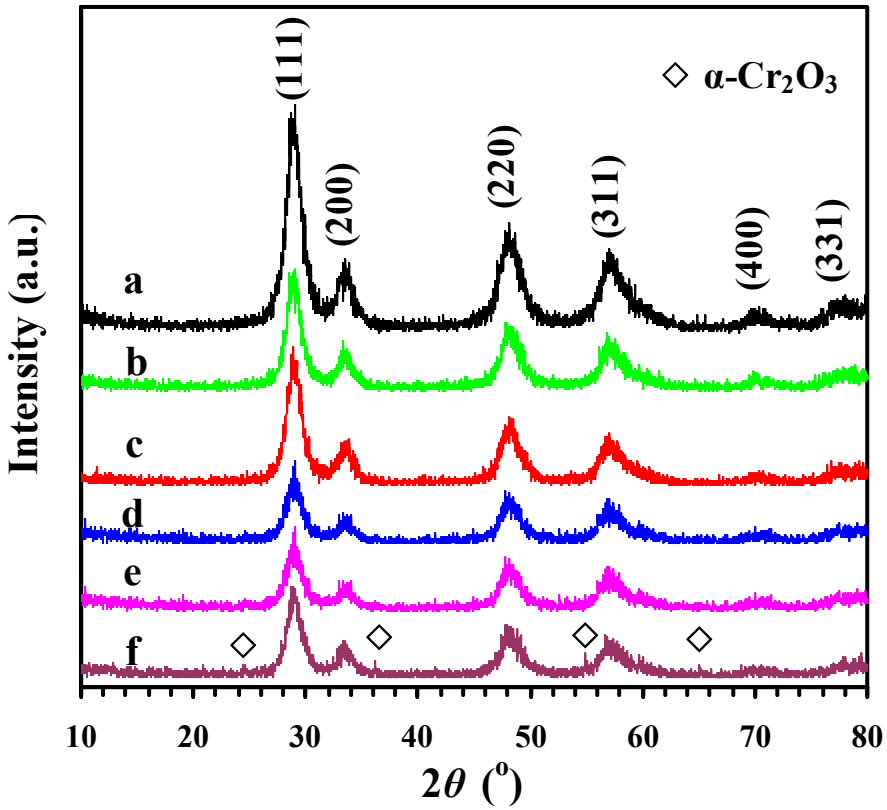

Fig. 1. XRD patterns of *y* CrO_x/*nano*-CZY samples with *y* = (a) 0, (b) 2, (c) 4, (d) 6, (e) 8, and (f) 10 wt%.

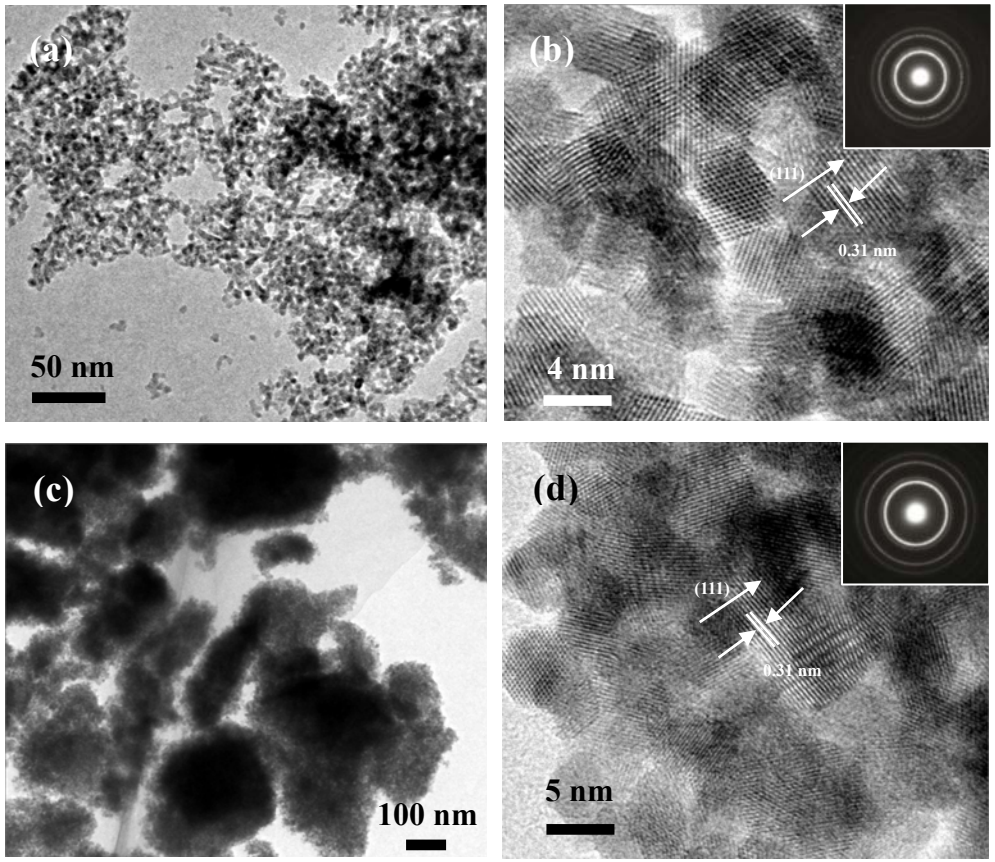

Fig. 2. TEM images and SAED patterns (insets) of (a, b) *nano*-CZY and (c, d) 8 wt% CrO_x/*nano*-CZY.

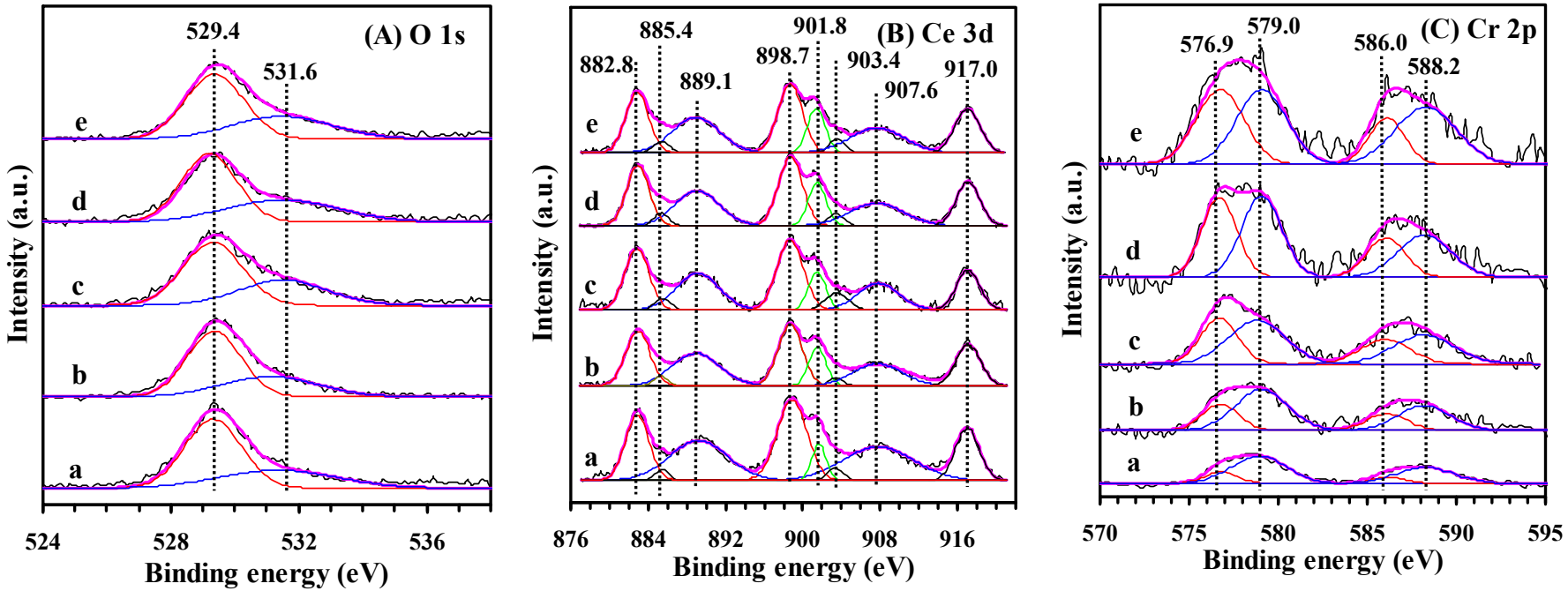

Fig. 3. (A) O 1s, (B) Ce 3d, and (C) Cr 2p XPS spectra of *y* CrO_x/*nano*-CZY with *y* = (a) 2, (b) 4, (c) 6, (d) 8, and (e) 10 wt%.

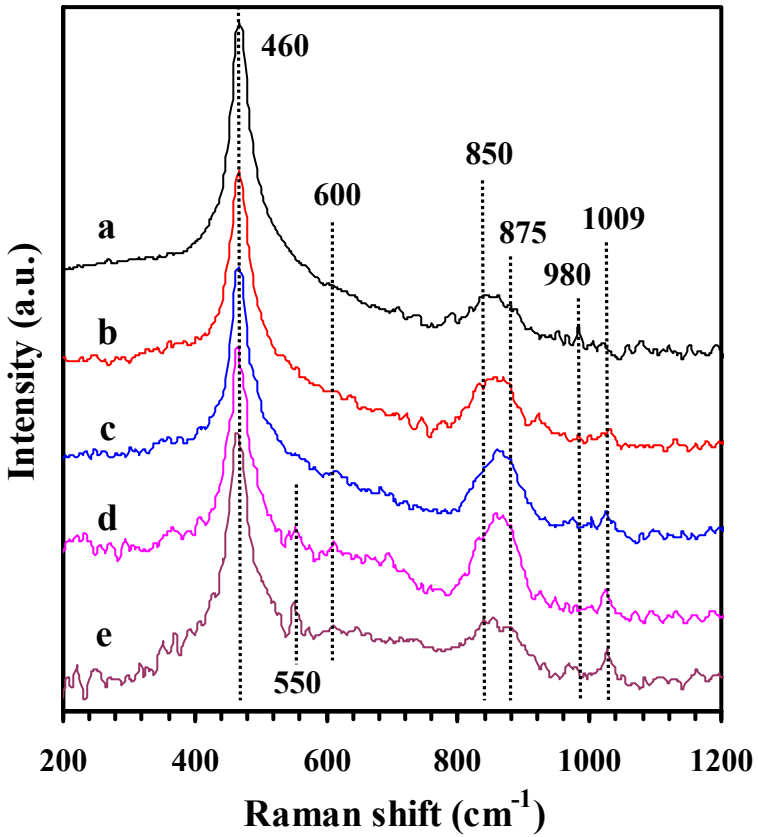

Fig. 4. Laser Raman spectra of *y* CrO_x/*nano*-CZY with *y* = (a) 2, (b) 4, (c) 6, (d) 8, and (e) 10 wt%.

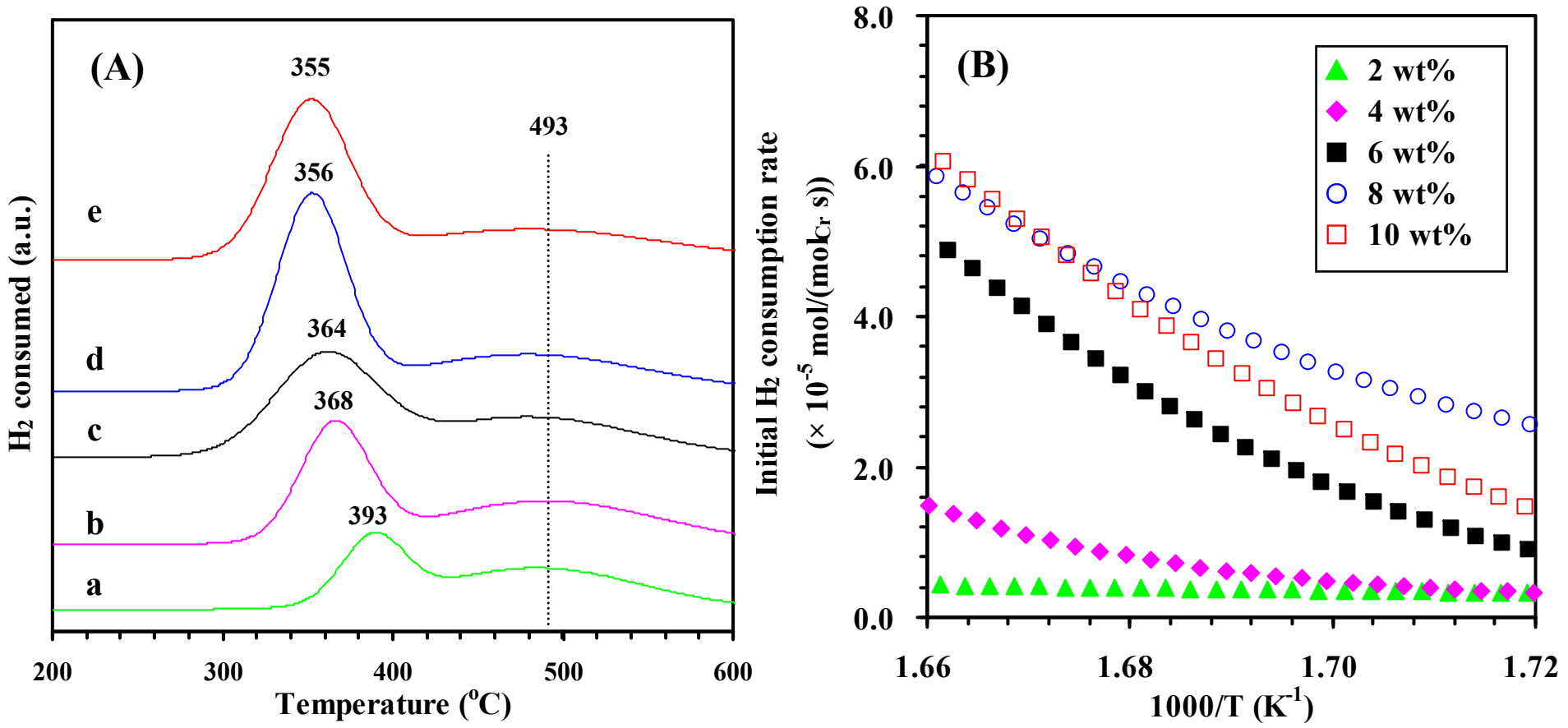

Fig. 5. (A) H_2-TPR profiles and (B) H_2 consumption rate of *y* CrO_x/*nano*-CZY with *y* = (a) 2, (b) 4, (c) 6, (d) 8, and (e) 10 wt%.